The Korean Journal of Rheology,
Vol. 10, No. 2, June 1998 pp. 98-105

<연구논문>

배향 타원체를 이용한 결정성 고분자의 배향특성 해석

우 종 표
명지대학교 공과대학 화학공학과
(1998년 4월 29일)

Analysis of Crystalline Polymer Orientation Via Representation of Orientation Ellipsoids

Jong-Pyo Wu
Dept. of Chemical Engineering, Myong Ji University,
Yongin, Kyonggi-do 449-728, Korea
(Received April 29, 1998)

요 약

가공공정중 변형을 수반하게되는 고분자제품은 대부분 고분자사슬의 배향(chain orientation)을 갖게된다. 이러한 사슬배향은 제품의 기계적, 광학적, 그리고 전기적 특성에 매우 중요한 영향을 미치는 것으로 알려져 있다. 지금까지 고분자사슬의 배향상태를 나타내기 위한 여러 방법은 모두 배향의 중심축들(principal axes)이 알려져 있다는 가정하에 전개되었다. 그러나 복잡한 배향모드를 갖는 고분자가공의 경우에 배향중심축이 실험축과 일치하지 않는 경우가 많다. 따라서 본 연구에서는 일반적인 고분자의 배향상태를 나타내는 방법에 대해 알아보고, 실제 고분자 가공공정에 적용을 위해 실험적으로 배향의 대칭축을 찾을 수 있는 접근방법을 제시하고자 하였다. 그 결과 결정성 고분자의 배향상태를 광각 x-선 회절 data를 이용한 2차 배향 tensor를 통해 배향 타원체를 구성할 수 있었다. 이를 PET 연신 필름 과 HDPE 사출성형물에 적용해 본 결과 이들의 2차 배향 tensor가 타원체를 잘 구성함을 알 수 있었다. 또한 주어진 고분자의 결정면들에 관계없이 고유한 중심축을 지니고 있음을 확인할 수 있었다. 이를 통해 복잡한 배향모드를 갖는 경우에 본 연구에서 제안한 X-타원체를 통해 결정의 배향 중심축을 효과적으로 찾을 수 있음을 알 수 있었다.

Abstract—Polymer products which experience deformation during processing generally result in molecular orientation. This molecular orientation affects the properties of products, such as their mechanical, optical, and elec trical properties significantly. To represent the state of orientation, we usually assume the directions of principal axes of orientation. However, in general, one does not have any information about the principal axes which can differ from the experimental axes in fabricated polymer parts. It is the purpose of this study to examine the general orientation descriptions and to develop the methodology for the experimental determination of principal axes of orientation. The orientation ellipsoid from the wide angle x-ray diffraction pole figure was developed. This ellipsoid was experimentally proven valid for the injection molded HDPE and biaxially stretched PET films. The principal axes in the ellipsoid indicate the unique directions irrespective of the different crystallographic planes. It is suggested that the ellipsoidal representation is useful in determining the unknown principal axes of orientation.
Keywords: molecular orientation, ellipsoid, semicrystalline polymer, wide angle x-ray diffraction

1. Introduction

Most polymer products which experience deformation during processing inevitably result in molecular orientation. It is known that this molecular orientation significantly affects the characteristics of products, such as their mechanical, optical, and electrical properties. For this reason there has been much effort to describe the state of orientation of polymer molecules[1-7].

Many different approaches certainly exist to represent the state of orientation of polymer chains such as a complete probability distribution function for the orientation of polymer chain segments and a more compact form of orientation factor. Though either approach has its own advantages, it usually relies on assumptions about the directions of principal axes of orientation. These assumptions are obvious in the cases of melt spun fibers and biaxially stretched or tubular blown films. The fiber axis in melt spun filaments and the machine, transverse, and normal directions in tubular blown or stretched films correspond to the principal axes of orientation. However, in general, one does not know the principal axes which can differ

from the experimental directions in fabricated parts which are usually presumed to represent the principal axes.

In this manuscript, we examined a general orientation description and the problems encountered in polymer processing, and developed experimental methodology to overcome this problems.

2. Theoretical analysis

Orientation Distribution Function and Orientation Factor.

The orientation distribution of structural units is a mathematical representation based on the appropriate coordinate system. One can use spherical harmonics with associated Legendre polynomials to represent the chain orientation distribution function based on the spherical coordinate system (r, φ, κ) with radius r, polar angle φ, and azimuthal angle κ. This approach has been carried out by Roe and Kigbaum[2] and Nomura et al.[3]. If one defines the normalized chain orientation distribution function θ(φ, κ) by

$$\int_0^{2\pi}\int_0^{\pi} \rho(\varphi, \kappa) \sin\varphi \, d\varphi \, d\kappa = 1. \tag{1}$$

Then this orientation distribution function can be expanded into a spherical harmonics as

$$\rho(\zeta, \kappa) = \sum_{l=0}^{\infty}\sum_{m=-l}^{l} Q_l^m \Pi_l^m(\zeta) e^{-im\kappa} \tag{2}$$

where $\Pi_l^m(\zeta)$ is normalized associated Legendre's polynomials, Q_l^m is the coefficients in the series expansion of orientation distribution function, and $\zeta=\cos\varphi$. The coefficients Q_l^m can be given by

$$Q_l^m = (1/2\pi) \int_0^{2\pi}\int_{-1}^{1} \rho(\varphi, \kappa)\Pi_l^m(\zeta) d\zeta d\kappa. \tag{3}$$

If one can determine values of the coefficient Q_l^m, one can obtain the orientation distribution function ρ(ζ, κ) using Eq.(2).

Suppose one imposes symmetry conditions on the orientation distribution functions as orthogonal biaxial symmetries with known principal axes of orientation, then the Q_l^m are non-zero for only even numbers of l and m. Consequently Eq.(2) becomes

$$\rho(\zeta, \kappa) = \sum_{l=0}^{\infty} Q_l^0 \Pi_l(\zeta) + 2\sum_{l=2}^{\infty}\sum_{m=2}^{l} Q_l^m \Pi_l^m(\zeta) \cos m\kappa. \tag{4}$$

In principle these approaches can be applied for the complete description of the orientation distribution function for the detailed texture of chain orientation. In a practical sense the main problem associated with this orientation distribution function is the experimental evaluation of the coefficients Q_l^m. Most available experimental techniques, including birefringence and infrared absorption measurements, are limited to only yield information on Q_2, and other measurements, including polarized fluorescence, Raman, and broad line NMR are limited to Q_4's.

Another approach to represent the orientation state is a compact form of the orientation factors which correspond to the specific moment of orientation average. These generalized orientation factors for the l-th moment, F_{lm}, can be expressed[3] based on Eq.(4)

$$F_{lm} = [2(l+m)!/(2l+1)(l-m)!]^{1/2}\Pi_l^m(\zeta)\cos m\kappa \tag{5}$$

Here l=0,2,4,6⋯,and m=0,2,⋯,l.

As mentioned above, there is no unique method for the representation of orientation. One may choose any coordinate system for their own conveniences and advantages. For the Euler coordinate system, there exists a strong advantage which results from a well-established mathematical formulation in that coordinate system. In the biaxial orientation state encountered in many polymer processing operations, it may be convenient to interchange two axes such as the machine and transverse directions. Representation of orientation using Euler coordinates seems inconvenient on this point.

Another coordinate system (φ_1, φ_2) which is associated with two polar angles has been used by several investigators[8,9] beginning with Wilchinsky[8] and Desper and Stein[11]. This coordinate system has its own advantage. The orientation factors obtained on this coordinate can be easily interchanged between the two axes. Biaxial orientation factors based on two polar angle coordinate systems have been developed by White and Spruiell[12]. They described second moment orientation factors based on the polarizability tensor. For a specific chain segment the polarizability along each direction 1, 2, and 3 can be used in the following biaxial orientation factors, f_{1c}^B and f_{2c}^B.

$$f_{1c}^B = (\overline{\alpha_{11}-\alpha_{33}})/(\alpha_{\parallel}-\alpha_{\perp}) = \overline{2\cos^2\varphi_{1c}} + \overline{\cos^2\varphi_{2c}} - 1 \tag{6a}$$

$$f_{2c}^B = (\overline{\alpha_{22}-\alpha_{33}})/(\alpha_{\parallel}-\alpha_{\perp}) = \overline{2\cos^2\varphi_{2c}} + \overline{\cos^2\varphi_{1c}} - 1 \tag{6b}$$

where $\alpha_{\parallel}$ is the polarizability along the chain axis, the $\alpha_{\perp}$ is the polarizability perpendicular to the chain axis, and φij is the angle between the laboratory axes(i) and chain axes(j). Biaxial orientation factors in Eq.(6) show obvious

symmetric character with respect to the 1 and 2 axes.

More notably, it can be readily extended to the complex orientation state such as unknown principal axes of orientation. Due to the nature of the second order tensor character of polarizability α_{ij}, it can always be transformed to their principal axes, I, II, and III.

$$\alpha_{ij} = \begin{bmatrix} \alpha_{11} & \alpha_{12} & \alpha_{13} \\ \alpha_{21} & \alpha_{22} & \alpha_{23} \\ \alpha_{31} & \alpha_{32} & \alpha_{33} \end{bmatrix} \Rightarrow \begin{bmatrix} \alpha_{I} & 0 & 0 \\ 0 & \alpha_{II} & 0 \\ 0 & 0 & \alpha_{III} \end{bmatrix} \tag{7}$$

This concept was applied by White and Cakmak[9] for the representation of orientation with unknown principal axes. Here the only and prerequisite problem in the characterization of orientation is the determination of the transformation angles for a unified view of chain orientation in fibers, films, and molded products.

Ellipsoidal Representation of Orientation. The representation of ellipsoid is particularly useful in interpretation of the principal axes of second order tensors including those which are useful to specify orientation. The polarizability is phenomenologically related to dielectric constants and through Maxwell's theory to refractive index. The polarizability tensor leads to a dielectric tensor and a refractive index tensor[13]. Fresnel's ellipsoid which represents refractive index can be written as follows:

$$\sum_i \sum_j n_{ij} x_i x_j = 1 \tag{8}$$

where n_{ij} is the refractive index tensor. For absorbing materials it can be shown that anisotropy leads to a similar absorption intensity ellipsoid[14] based on specific chain segments of a molecule. One can express this absorption ellipsoid as:

$$\sum_i \sum_j A_{ij} x_i x_j = 1 \tag{9}$$

where A_{ij} is the absorption intensity tensor. The refractive index ellipsoid represents an integral property of amorphous and crystalline phase, while the infrared absorption ellipsoid represents a selective property for a specific segment of the molecule.

On the other hand the pole figure from wide angle x-ray diffraction represents a distribution of plane normals of specific crystallographic planes. The pole figure inherently reveals the detailed texture of orientation of the crystalline phase, i.e., it implies the orientation information of the higher order such as the second moment, etc.. If the second order tensorial quantity, which is related to specification of crystalline orientation, can be developed from the pole figures of wide angle x-ray diffraction, it will play an important role in the experimental determination of principal axes of crystalline orientation.

One can apply the concept of analogy between the plane normal vector in wide angle x-ray diffraction and the transition moment vector in infrared absorption to develop a new quantity[14]. Consider coordinate systems as shown in Fig. 1. In one of them the axes a, b, and c are adapted to a unit cell of the polymer crystal, the axes 1, 2, 3 are laboratory axes, while the axes I, II, III are the principal coordinate system. Suppose a plane normal vector N has the three component N_a, N_b, N_c in the unit cell coordinate system, then the components N_I, N_{II}, N_{III} are given by

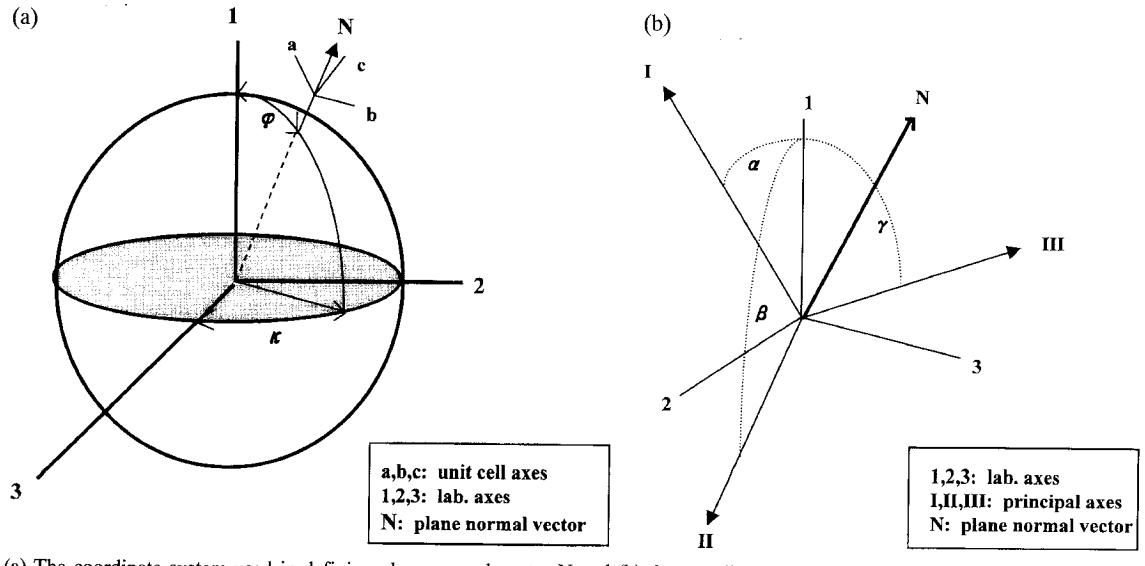

Fig. 1. (a) The coordinate system used in defining plane normal vector N and (b) the coordinate system used in deriving x-ellipsoid.

$$N_{I,\ II,\ III} = T\,N_{a,\ b,\ c} \tag{10}$$

where T is the second order tensor which correlates the transformation between the polymer unit cell coordinate and the principal coordinate system. When one performs the pole figure experiment, where the arbitrary machine direction(lab. axis 1 in Fig. 1) in the pole figure is maintaining specific polar angles α, β, γ with respect to principal coordinate system I, II, III as shown in Fig. 1, each component N_I, N_{II}, N_{III} of the individual plane normal is involved in the determination of averaged cosine square and its value is proportional to $N^2_{\alpha,\ \beta,\ \gamma}$. Since the distribution function $I(\varphi, \kappa)$ obtained from the pole figure experiment corresponds to the number of plane normals pointing to the specific segment, the averaged cosine square value, $X_{\alpha,\ \beta,\ \gamma}$ which representing $\overline{\cos^2\varphi_{\alpha,\ \beta,\ \gamma}}$ is given by

$$X_{\alpha,\ \beta,\ \gamma} = \frac{\iint I(\varphi,\ k)\sin\varphi\, N^2_{\alpha,\ \beta,\ \gamma}\, d\varphi d\kappa}{\iint I(\varphi,\ k)\sin\varphi\, d\varphi d\kappa} \tag{11}$$

where $X_{\alpha,\ \beta,\ \gamma}$ is the averaged cosine square value obtained from the arbitrarily chosen machine direction in the pole figure experiment as shown in Fig. 1. On the other hand, the component of the individual plane normal in arbitrary direction (α, β, γ) in Fig. 1 is given by

$$N_{\alpha,\ \beta,\ \gamma} = N_I\cos\alpha + N_{II}\cos\beta + N_{III}\cos\gamma \tag{12}$$

The Eq.(11) and (12) result in

$$X_{\alpha,\ \beta,\ \gamma} = X_I\cos^2\alpha + X_{II}\cos^2\beta + X_{III}\cos^2\gamma + 3\ \text{cross-terms} \tag{13}$$

Due to the symmetry of $I(\varphi, \kappa)$, the last 3 cross-terms in Eq.(13) are equal to zero. The Eq.(13) represents the equation of the ellipsoid obtained from the plane normal distributions. Now we can generalize the $X_{\alpha,\ \beta,\ \gamma}$ in the form of a second order tensor as

$$X_{ij} = \overline{\cos\varphi_i\ \cos\varphi_j} = \frac{\iint I(\varphi,\ \kappa)\sin\varphi\, N_i N_j\, d\varphi d\kappa}{\iint I(\varphi,\ \kappa)\sin\varphi\, d\varphi d\kappa} \tag{14}$$

The ellipsoid of X_{ij} can then be expressed in simple form on the appropriate space coordinate system.

$$\sum_i \sum_j X_{ij}\, x_i\, x_j = 1 \tag{15}$$

$$X_I\, x_I^2 + X_{II} x_{II}^2 + X_{III} x_{III}^2 = 1 \tag{16}$$

where I,II, and III represent principal axes. The schematic representation of the X ellipsoid is shown in Fig. 2.

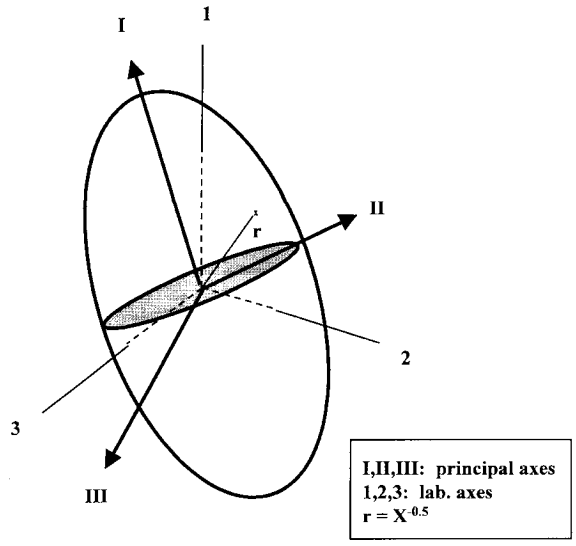

Fig. 2. Schematic representation of X ellipsoid.

3. Experimental section

Wide angle x-ray pole figure experiments were carried out using an x-ray generator equipped with a single crystal orienter by General Electric(Model XRD-6) with a copper target and Ni-β filter(λ=1.542Å). The operating voltage and current were 40 KV and 50 mA, respectively.

The materials used in this study were high density polyethylene(HDPE, DuPont Alathon 7050), poly(ethylene terephthalate)(PET, Eastman Kodak Co. Tenite 7352). The samples which had anisotropic molecular orientation were prepared by injection molding machine(Boy Model 15-S) for HDPE and biaxial film stretching machine(Iwamoto Model BIX-702) for PET. The specimens with dimension of 1.0 mm × 1.0 mm × 1.5 mm were mounted on the single crystal orienter which could be tilted up to 90° and rotated up to 360°. Before beginning the pole figure experiments, a 2θ scan was performed and diffractometer was set to the maximum 2θ peak of each crystallographic diffraction planes. The planes used in this experiment were (110), (200), and (020) planes for HDPE and (010), (100), and (-105) planes for PET. The data acquisition is automated with step scanning φ from 0° to 90° in 5° intervals and κ from 0° to 360° in every 10°. Therefore 665 data points of WAXD intensity on each specific crystallographic plane were obtained in the pole figure experiment.

4. Results

To apply X ellipsoid from the pole figure data, it is necessary to obtain a complete set of $X_{\alpha,\ \beta,\ \gamma}$ data for all the

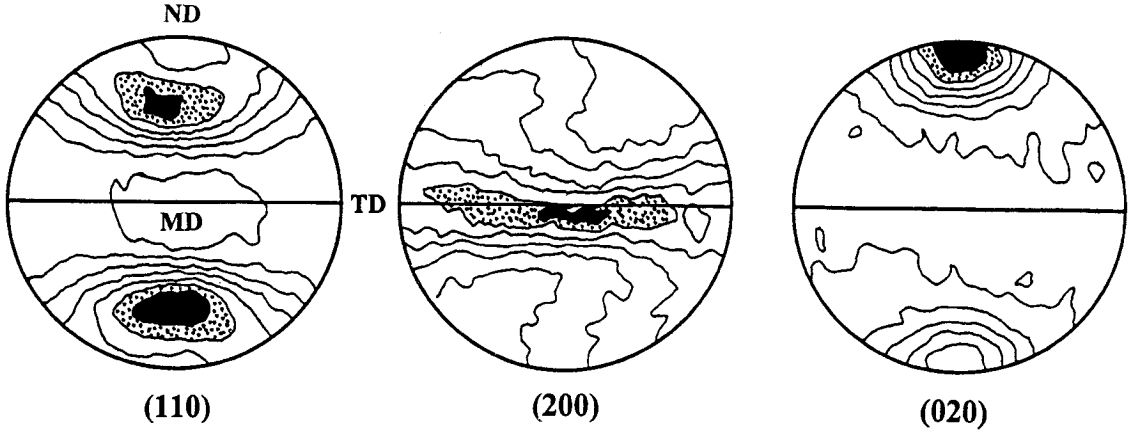

Fig. 3. The wide angle x-ray diffraction pole figures of injection molded HDPE. (melt/mold temp.=160°C/25°C, injection speed=106.1 cm^3/sec, holding pressure=$1.38\times10^6 N/m^2$, center gated $3.175\times12.7\times127$ mm rectangular test mold; sample was cut from the mold wall region; MD, ND and TD represent flow, thickness and width directions, respectively)

possible α, β, γ combinations. However, it is impractical to obtain those values experimentally for the every α, β, and γ. In this sense it is useful to transform the experimental pole figure intensity distribution data I(φ, κ), obtained at the specific fixed direction, to the I'(φ', κ') for the arbitrary α, β, γ direction. The data was transformed to each step of angle φ and κ with the intervals of 5° and 10°, respectively. Then the $X_{\alpha,\beta,\gamma}$ value at each corresponding α, β, γ combinations was calculated using Eq.(11).

The wide angle x-ray diffraction pole figures of injection molded HDPE which has orthorhombic crystal unit cell structure are shown in Fig. 3. Here MD represents the direction of flow, TD and ND correspond to the width direction and thickness direction, respectively. The results indicated by these pole figures imply that the (110) plane normal direction is located mainly between the flow direction and the thickness direction. They also imply that the highest intensity of the (020) plane normal is placed at the thickness direction. The values of $X_{\alpha,\beta,\gamma}$ along the MD(flow direction)-ND(thickness direction) calculated by Eq.(11) are listed in Table 1. According to the Eq.(16), the $X^{-0.5}$ values in the spatial coordinate system must represent the ellipsoid. We plot the experimental values of $X^{-0.5}$ in a polar diagram as shown in Fig. 4, where the dots represent the experimental data and the solid curve was obtained by the linear regression of the general equation of ellipsoid. Due to the geometric symmetry of the processing system used in this study, the two dimensional ellipse instead of three-dimensional ellipsoid was presented. It is surprising to note that the experimental results follow the ellipses well enough irrespective of the different crystal planes of HDPE. The deviations of experimental data were found to be limited to the range of ± 0.42%. This supports the X ellipsoid developed in this study using wide angle x-ray diffraction. Furthermore the experimentally determined principal axes of crystalline orientation from Fig. 4 indicate the unique directions irrespective of the different crystallographic planes.

On the other hand, the wide angle x-ray diffraction film patterns for nonorthogonally biaxially stretched PET films which have triclinic crystal structure are shown in Fig. 5.

Table 1. The calculated $X_{\alpha,\beta,\gamma}$ values of injection molded HDPE (melt/mold temp.=160°C/25°C, injection speed=106.1 cm^3/sec, holding pressure=$1.38\times10^6 N/m^2$, center gated $3.175\times12.7\times127$ mm rectangular test mold; sample was cut from the mold wall region; the angle represents the angle between the arbitrary direction with respect to flow direction in the plane of flow direction -thickness direction)

X value / Angle(°)	$X_{\alpha,\beta,\gamma}$ (110) Plane	(200) Plane	(020) Plane
0	0.2012	0.4378	0.2072
10	0.2150	0.4170	0.2218
20	0.2457	0.3854	0.2553
30	0.2924	0.3417	0.3009
40	0.3512	0.2907	0.3525
50	0.4125	0.2369	0.4050
60	0.4682	0.1870	0.4521
70	0.5114	0.1480	0.4887
80	0.5377	0.1368	0.5089
90	0.5435	0.1238	0.5094
100	0.5226	0.1467	0.4925
110	0.4889	0.1813	0.4616
120	0.4396	0.2261	0.4190
130	0.3808	0.2807	0.3688
140	0.3198	0.3330	0.3170
150	0.2670	0.3794	0.2704
160	0.2279	0.4149	0.2322
170	0.2059	0.4347	0.2101
180	0.2012	0.4378	0.2072

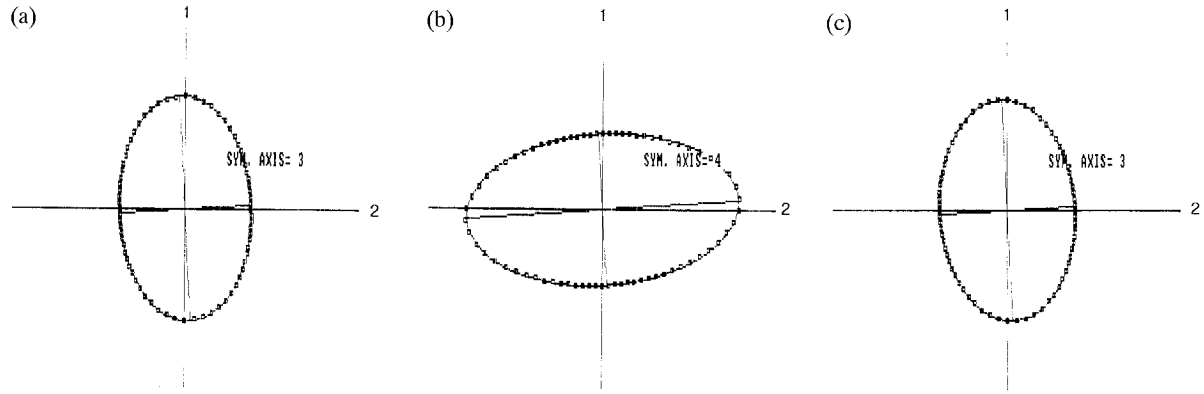

Fig. 4. The X ellipsoids for the different crystallographic planes of injection molded HDPE. (a) (110) plane, (b) (200) plane and (c) (020) plane. (lab. axis 1 and 2 represent flow direction and thickness direction)

Fig. 5. Wide angle x-ray diffraction patterns of nonorthogonally biaxially stretched PET film. (1st/2nd stretch ratio=3.0/1.5, stretching temp.=90°C, annealed at 150°C, skew angle=60°; x-ray beam enters to the normal to the film surface and the vertical direction corresponds to the second stretching direction)

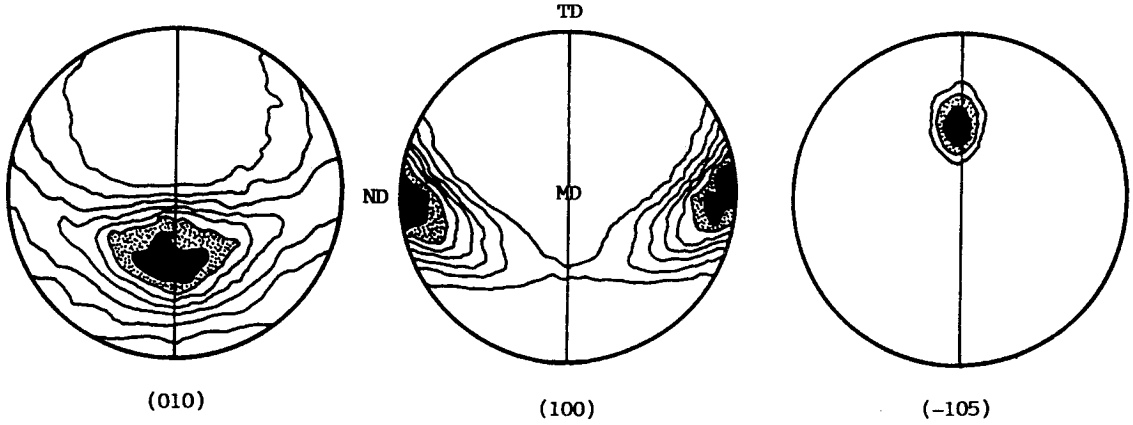

Fig. 6. The wide angle x-ray diffraction pole figures of stretched PET films. (1st/2nd stretch ratio=3.0/1.5, stretching temp.=90°C, annealed at 150°C, skew angle=60°; MD and ND represent the second stretching direction and the normal to the film direction)

They reveal distinctive asymmetric diffraction patterns with respect to a certain laboratory direction. From these diffraction patterns alone it is very difficult to understand the orientation state of specific crystallographic planes. To represent the specific texture of orientation for each specific crystallographic planes, wide angle x-ray diffraction of

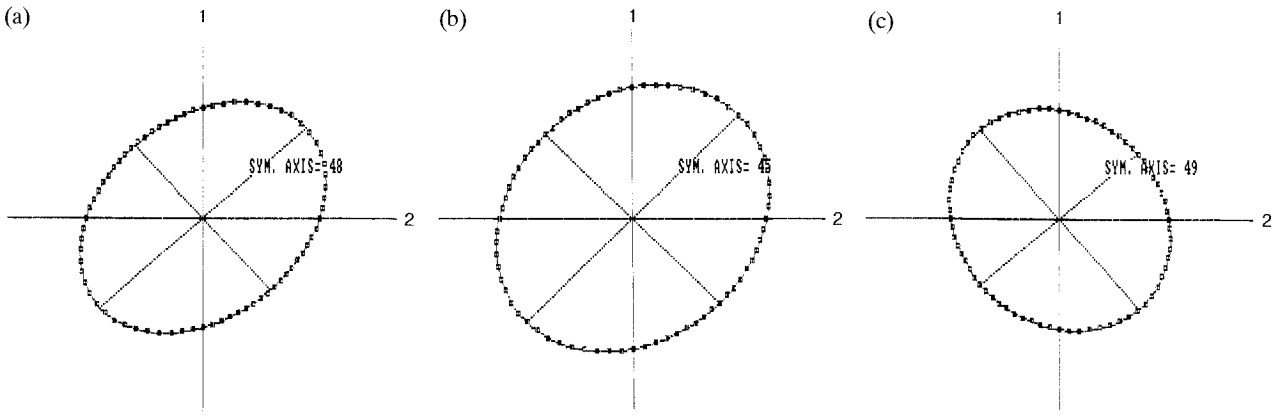

Fig. 7. The X ellipsoids for the different crystallographic planes of stretched PET films. (a) (010) plane, (b) (100) plane and (c) (-105) plane.(lab. axis 1 and 2 represent the second stretching direction and the perpendicular to the second stretching direction)

the PET films are presented in terms of pole figures as shown in Fig. 6. The (-105) plane normal is parallel to the chain axis. The (100) plane normal is nearly perpendicular to the aromatic rings in the PET. The (010) plane makes angles of 80° and 59° to the (-105) and (100) planes, respectively. In this figure MD represents the second stretching direction and ND represents the film thickness direction. In Fig. 6, the strong diffraction intensity for the (010) plane is in the MD-TD plane. For the (100) plane which gives information on aromatic ring orientation, the diffraction intensity is focused at ND. For the (-105) plane which gives an idea of chain orientation, the highest diffraction intensity is located in the MD-TD plane. These suggest that two of principal axes of PET films are located in the MD-TD plane and the other symmetry axis is parallel to the film thickness direction. We also plot the experimental values of $X^{-0.5}$ as shown in Fig. 7. The deviations of experimental data were limited to the range of $\pm 0.20\%$. This again supports the concept of X ellipsoid developed in this study.

The results of X ellipsoid obtained from the pole figure data are summarized in Table 2. For complexly oriented products such as injection molded parts or biaxially stretched films of semicrystalline polymers, this X ellipsoid can be successfully applied in determining the principal axes of orientation for crystalline orientation.

Table 2. Summarized results of X ellipsoid obtain from the pole figure data

Material	Crystal structure	Plane	Least square error(%)	Principal axis angle*(°)
HDPE	Orthorhombic	(110)	0.35	3
		(200)	0.42	4
		(020)	0.18	3
PET	Triclinic	(010)	0.13	48
		(100)	0.20	45
		(-105)	0.20	49

*)The angle between the major principal axis of orientation and the lab. axis 1 (the lab. axis 1 corresponds to the flow direction for injection molded HDPE and the second stretching direction for PET film)

5. Conclusions

We have examined the general orientation descriptions and the problems encountered in the description of orientation in fabricated polymer parts. It was found that the prerequisite step in the characterization of complexly oriented polymer materials is the experimental determination of the unknown principal axes. The ellipsoidal representation might be useful in determining the unknown principal axes.

The X ellipsoid from the pole figure of wide angle x-ray diffraction was developed based on the phenomenological analogy between the transition moment vector in absorptivity and the plane normal vector in wide angle x-ray diffraction.

This ellipsoid was experimentally proven valid for various crystallographic planes of polymers and also confirmed irrespective of the different crystallographic unit cell structures of each polymer. The principal axes in the X ellipsoid indicate the unique direction irrespective of the different crystallographic planes.

Acknowledgement

This research was supported in part by research fund(1998) from Regional Research Center at Myong Ji University.

References

1. J.J. Hermans, P.H. Dermans, D. Vermaas and A. Weidinger, *Rec.*

Trav. Chim., **65**, 427 (1946).
2. R.J. Roe and W.R. Krigbaum, *J. Appl. Phys.*, **36**, 2004 (1965).
3. S. Nomura, H. Kawai, I. Kimura and S. Kagiyama, *J. Polym. Sci.*, **5**, 479 (1967).
4. J.L. White, *Pure Appl. Chem.*, **55**, 765 (1983).
5. H.J. Wolter, G.Vancso, I. Tomka and J. Meissner, *Polym. Bulletin*, **19**, 389 (1988).
6. M. Kosc, *Colloid & Polym. Sci.*, **270**, 106 (1992).
7. P. Lapersonne, D.I. Bower and I.M. Ward, *Polym.*, **33**, 1277 (1992).
8. J.L. White, *J. Polym. Eng.*, **5**, 275 (1985).
9. J.L. White and M. Cakmak, *Int. Polym. Proc.*, **2**, 48 (1987).
10. Z.W. Wilchinsky, *J. Appl. Polym. Sci.*, **7**, 923 (1963).
11. C.R. Desper and R.S. Stein, *J. Appl. Phys.*, **37**, 3990 (1966).
12. J.L. White and J.E. Spruiell, *Polym. Eng. Sci.*, **21**, 859 (1981).
13. M. Born and N.E. Wolf, "Principles of Optics", 4th Ed., Pergamon, London, 1970.
14. R. Zbinden, "Infrared Spectroscopy of High Polymer", Academic Press, N.Y., 1964.